

Feasibility of ultrasound phase contrast for heating localization

Caleb H. Farny^{a)} and Greg T. Clement

Department of Radiology, Harvard Medical School, Brigham and Women's Hospital, Boston, Massachusetts 02115

(Received 8 August 2007; revised 20 December 2007; accepted 22 December 2007)

Ultrasound-based methods for temperature monitoring could greatly assist focused ultrasound visualization and treatment planning based on sound speed-induced change in phase as a function of temperature. A method is presented that uses reflex transmission integration, planar projection, and tomographic reconstruction techniques to visualize phase contrast by measuring the sound field before and after heat deposition. Results from experiments and numerical simulations employing a through-transmission setup are presented to demonstrate feasibility of using phase contrast methods for identifying temperature change. A 1.088-MHz focused transducer was used to interrogate a medium with a phase contrast feature, following measurement of the baseline reference field with a hydrophone. A thermal plume in water and a tissue phantom with multiple water columns was used in separate experiments to produce a phase contrast. The reference and phase contrast field scans were numerically backprojected and the phase difference correctly identified the position and orientation of the features. The peak temperature reconstructed from the phase shift was within 0.2 °C of the measured temperature in the plume. Simulated results were in good agreement with experimental results. Finally, employment of reflex transmission imaging techniques for adopting a pulse-echo arrangement was simulated, and its future experimental application is discussed.

© 2008 Acoustical Society of America. [DOI: 10.1121/1.2835438]

PACS number(s): 43.80.Qf, 43.35.Bf, 43.80.Ev, 43.35.Yb [FD]

Pages: 1773–1783

I. INTRODUCTION

Noninvasive, inexpensive, and prompt visualization of temperature rise remains a significant barrier to optimizing thermal therapies for cancer tissue ablation such as high-intensity focused ultrasound (HIFU), radio-frequency (rf) ablation, and cryoablation. Variability in tissue structure between patients and target movement during treatment makes it difficult to predict *a priori* where and how much energy will be deposited in the treatment region, so treatment time and outcome can suffer greatly without adequate visualization and guidance. For HIFU treatment, measurement of the proton resonant frequency shift with magnetic resonance (MR) imaging is the current gold standard^{1,2} for monitoring thermal damage but there is a clear motivation for a cheaper, portable method with higher temporal and spatial resolution. Each of these requirements contributes to an ongoing investigation of ultrasound-based thermographic methods. A number of other applications ranging from nondestructive testing^{3,4} to meteorology^{5,6} have a similar need for noninvasive, portable methods of temperature measurement.

Nearly all ultrasound methods for measuring temperature rise in tissues are based on empirical relationships for sound speed and temperature for various tissue types. Similar to water, the sound speed for most tissue types increases approximately quadratically with temperature but exhibits an inflection point near 70 °C and decreases for higher temperatures; the sound speed of some tissues types, such as fat, instead decreases with increasing temperature.⁷ Based on these relationships, knowledge of local sound speed will

yield the local temperature. A drawback to this approach occurs when multiple tissue types having varying dependencies on temperature are present in the measurement volume, resulting in an approximation of the actual temperature. However, although a direct measurement of the *in vivo* temperature remains an important goal for treatment guidance, an intermediate goal of simply localizing the beam focus relative to the target would greatly improve treatment efficacy. A method designed to locate the focus rather than quantify temperature rise justifies use of a homogeneous approximation for the tissue structure, allowing a single relationship between sound speed and temperature. A short, low-power sonication has been employed as a “citing shot”^{8,9} before the therapeutic sonication is applied, for the sole purpose of determining the position of the focus *in vivo*.

A number of ultrasound-based techniques take advantage of standard ultrasound diagnostic imaging platforms for measuring sound speed change. Commonly, the spatial dimensions on which a diagnostic image is based assume that the medium corresponds to a uniform 1540 m/s sound speed, that of normal body temperature. Under this assumption, an increase in temperature will shift the image, and by comparing the apparent spatial shift with an initial (unheated) image,^{13–19} the sound speed change can be determined.^{13–19} A second phenomenon which will occur is thermal expansion, which results in a physical shift in the tissue.^{9,11–13,19}

Seip and Ebbini¹⁰ used the spectrum of the measured backscattered rf signal to track heating. Based on the change in the average tissue scatterer spacing from thermal expansion and the sound speed dependence on temperature, it was found that the shift in the resonance peak of the rf signal was

^{a)}Electronic mail: cfarny@bwh.harvard.edu

linearly proportional with the change in temperature. The technique was shown to agreeably estimate temperature rises for *in vitro* tissue samples up to 10 °C for waterbath heating and up to 4 °C for the cooling curve in *in vivo* ultrasound-heated tissue samples. However, it was theorized that higher temperature changes and resulting tissue damage would disrupt the scatterer structure on which the technique was based. Maass-Moreno and Damianou¹¹ and Maass-Moreno *et al.*¹² interlaced diagnostic and therapeutic ultrasound pulses to track heating in excised turkey breast. Cross-correlation techniques were used to determine the time change in the backscattered diagnostic signal. Linear approximation of the sound speed with temperature produced accurate temperature measurements for elevations up to 10 °C but estimations of higher temperature rises suffered.

Simon *et al.*¹³ correlated the backscattered ultrasound images as the temperature in tissue phantoms was increased, and found that the axial derivative of the successive echo shifts was proportional to temperature rise. The results reliably estimated temperature rises up to ~4 °C but it was found that spatial ripples introduced by a thermoacoustic lensing effect degraded the image. Two-dimensional low-pass filtering reduced the ripples but reduced spatial resolution as well. A number of other groups^{14–17} have successfully applied similar approaches, but primarily only in *in vitro* samples experiencing low (<10 °C) temperature rises. Varghese *et al.*^{18,19} showed success in measuring temperature change for *in vitro* and *in vivo* tissue samples for temperature elevations up to 100 °C from rf ablation therapy. The group cross-correlated rf ultrasound echo signals to determine the apparent time shift, despite applying a linear approximation for the sound speed relationship with temperature. It was theorized that the success of the resulting two-dimensional (2D) temperature map even at high temperatures was partly due to thermal expansion effects which were not explicitly accounted for in the analysis.

King *et al.*²⁰ used a different approach for measuring thermal effects. An acoustic camera equipped with a 128 × 128 polyvinylidene difluoride (PVDF) sensing array was positioned in a through-transmission arrangement with a planar 10 MHz transducer operated in pulse mode. *Ex vivo* rabbit liver and bovine fat tissue samples were instrumented with a thermocouple and sonicated with a high-power focused ultrasound source in order to induce temperature rises up to 100 °C. It was found that image intensity from the acoustic camera correlated well with the cooling curve in the sample following therapeutic sonication, and the lesion size measured from the intensity image correlated well with lesion sizes determined from histology. The authors theorized that the local change in sound speed caused a sufficient change in phase, altering the intensity on which the image was based. The technique offered a real-time measurement of temperature change but due to its insensitivity to different trends in the sound speed–temperature relationship of different tissue types, the resulting image was thought to be best suited for localization of the focus.

Based on the findings by King *et al.*,²⁰ it is theorized that by measuring phase shift, the change in sound speed and thus, change in temperature can be determined. Comparing

the change in phase angle between an unheated reference and subsequent heated wave can determine a change in sound speed, which is contained in the phase angle of the received sound wave. A similar approach was taken by Mizutani *et al.*²¹ and Ishikawa *et al.*,²² who applied ultrasound computed tomography (CT) techniques to measure the local time of flight at multiple positions through a region heated approximately 5–15 °C in air. A through-transmission setup was linearly and rotationally scanned around the target region so that the change in sound speed at multiple locations was known. Using an empirical relationship to determine temperature from sound speed, a filtered backprojection method was used to reconstruct the temperature rise to within 1 °C of the thermocouple-measured temperature.

It is proposed that reflex transmission imaging (RTI), planar projection, and tomographic methods can be applied to reconstruct a 2D map of sound speed and corresponding temperature rise from the change in phase angle, in a method that would not depend on speckle-tracking and correlation methods. RTI is a technique which has been used to improve backscattered *B*-mode image quality of attenuating media such as kidney stones embedded in soft tissue^{23,24} and skin tumors.²⁵ Typically, a diagnostic ultrasound imager is modified so that the signal reflected from a region beyond the focus is integrated. The principle is based on the fact that the integrated signal will depend on the characteristics of the return path length, which includes the focal zone, and can be treated as a virtual source, emulating a through-transmission setup. It is desirable to use a pulse-echo arrangement as opposed to through-transmission due to the limited number of acoustic windows in the body. Planar backward projection techniques in combination with tomographic reconstruction have been employed in transmission imaging simulations to visualize 2D temperature maps from phase contrast measurements.²⁶ It is noted that phase measurements often feature a higher signal-to-noise ratio than traditional backscattered ultrasound.

Interest here lies in understanding whether phase contrast from backprojection of the beam measured through an unheated and subsequent heated medium can be used to locate and measure the region of heating. In this feasibility study, a through-transmission arrangement was used and planar backprojection and tomographic reconstruction methods were employed to experimentally and numerically localize temperature rise and/or sound speed contrast from the change in phase angle. To apply this technique, it is necessary to measure the amplitude and phase of the sound field throughout a 2D plane with sufficient spatial resolution to properly backproject the beam. Therefore, two separate experimental arrangements featuring quasi-steady-state phase contrasts were employed due to the lengthy measurement time. The first arrangement used a thermal plume to produce a phase contrast, whereas the second arrangement consisted of a tissue phantom with multiple water columns. Finally, extension of the through-transmission approach to RTI was simulated in a pulse-echo arrangement, and future experimental employment is discussed.

II. THEORY

A. Phase angle

The relationship between sound speed and temperature is well-known for water and has been measured for a number of tissue types.⁷ The heating in the experiments was conducted in water, and a sixth-order fit of the measured relationship in water²⁷ was used to determine the corresponding sound speed. The sound speed is contained in the complex argument of the pressure wave, so by determining sound speed, the temperature can be found. If the reference sound speed c_0 is known, the change in sound speed can be determined from the difference in phase $\Delta\Phi$, where

$$\Delta\Phi = \omega z \left(\frac{1}{c_h} - \frac{1}{c_0} \right), \quad (1)$$

where ω is the angular frequency, z is the distance over which the contrast occurs, and c_h is the sound speed in the heated region.

B. Planar projection

Forward and backward planar projection techniques²⁸ are a computationally efficient method for determining the sound field at a different plane provided the amplitude and phase of the field and medium characteristics are adequately known. Each point of the field is treated as an individual plane wave and a propagation operator in 2D wave vector space can be used to model the phase at the new point in space, thereby projecting the entire field to the new plane. The relationship between the initial field P_i and projected field P_0 in wave vector space is

$$P_0(k_x, k_y, z) = \frac{1}{2\pi} \int \int P_i(k_x, k_y, z_i) \exp\left(i(z_0 - z_i) \times \sqrt{\frac{\omega^2}{c^2} - k_x^2 - k_y^2}\right) dk_x dk_y, \quad (2)$$

where k_x and k_y are the wave numbers and the exponential term is the transfer function propagation operator. The effects of evanescent waves, which are small for sufficiently large distances ($dz > \lambda$), must be set to zero to avoid buildup of numerical error for back projection.²⁹

C. Tomographic reconstruction

The experimental arrangement used here permitted for only one angle of interrogation of the medium, as opposed to rotation of the transmitter and receiver around the target commonly employed in CT imaging. In order to comply with this restriction, the measurements specifically used axially symmetric targets, allowing application of the Fourier slice theorem to reconstruct the distribution of heat throughout the target region. The 2D Fourier transform of an object $p(x, y)$ is defined as

$$P(k_x, k_y) = \int_{-\infty}^{\infty} \int_{-\infty}^{\infty} p(x, y) \exp(i(k_x x + k_y y)) dk_x dk_y. \quad (3)$$

The Fourier slice theorem states that a Fourier transform of a projection along an angle θ ,

$$P_{\theta}(x) = \int_{-\infty}^{\infty} p(x, y) dy, \quad (4)$$

is equivalent to a slice through the origin in wave vector space.³⁰ For a radially symmetric object such as a plume, the phase is no longer dependent on y , reducing the integral to

$$P(k_x, 0) = \int_{-\infty}^{\infty} P_{\theta=0}(x) \exp(ik_x x) dk_x. \quad (5)$$

This relationship reconstructs the 2D temperature distribution by taking the one-dimensional Fourier transform of the phase difference across the plume, rotating it about the origin in wave vector space and taking the 2D inverse transform.

III. MATERIALS AND METHODS

A. Experimental setup

Experiments were conducted in a tank lined with absorbing rubber pads and filled with deionized water. Interrogation of the medium was conducted by a focused transducer driven at its 1.088 MHz center frequency (50 mm diameter, 100 mm focal length) and the field at the focus was measured with a needle hydrophone and preamplifier (0.2 mm diameter, Precision Acoustics, Dorchester, UK). A function generator (396, Fluke Corp., Everett, WA) supplied the pulse train (35 cycles, 2 kHz pulse repetition frequency) which was amplified (240L, E & I Ltd., Rochester, NY) before passing through a matching network to the transducer. The hydrophone was scanned in a raster pattern with a 0.2 mm step size by a computer-controlled positioning system (VP9000, Velmex, Inc., Bloomfield, NY). The signal was digitized with an 8-bit oscilloscope (TDS 210, Tektronix, Inc., Richardson, TX), averaged, and transferred via GPIB for storage on the local computer. Data acquisition and analysis was performed with MATLAB (The MathWorks, Natick, MA). Due to the large measurement field and averaging time, the scan duration was several hours. Each measurement consisted of a reference scan of the homogeneous medium and a ‘‘heated’’ scan that contained the phase contrast in the sound path. The temperature of the water in the reference scans was monitored before and immediately following the scan and the sound speed in the analysis and corresponding simulation was based on the measured ambient water temperature.

Two separate setups were employed to produce a phase-contrast: a thermal plume and a tissue phantom. In order to simulate a thermal effect from a HIFU source but also comply with the steady-state time restriction, a heater was encased in thermal insulation with an open column in the top to produce a thermal plume, shown in Fig. 1(a). The reference scan consisted of measuring the field with the heater off and the heated scan was performed with the heater turned on. The thermal plume was positioned approximately 24 mm in

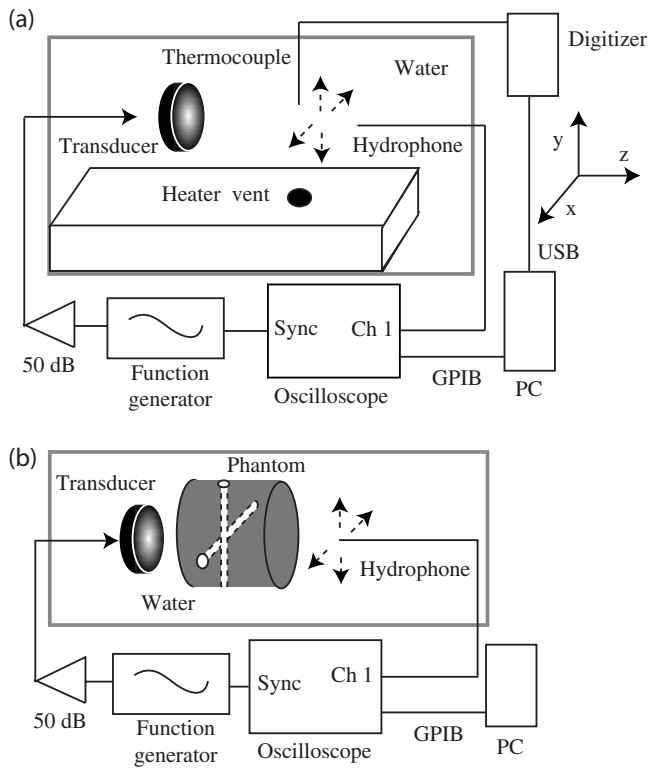


FIG. 1. Experimental arrangement for the phase contrast from (a) a thermal plume and (b) a tissue phantom intersected by water columns.

front of the focus and a thermocouple (type T, 50- μm wire diameter) was positioned in line with the hydrophone in the center of the plume to monitor the temperature in the plume along the sound path. At each position in the scan three thermocouple measurements were digitized (24 bit, NI-9211A, National Instruments Corp., Austin, TX) and averaged following transfer to the computer via USB. The thermocouple tip was positioned approximately 5 mm above the hydrophone x - z plane to minimize interference with the sound propagation. The sound field was measured with and without the thermocouple present and its presence did not exhibit a significant impact on the field. Maximum steady-state temperatures in the plume ranged from 5 to 15 $^{\circ}\text{C}$ above the reference temperature. Radial symmetry of the temperature distribution in the plume was determined by scanning the thermocouple across the acoustic (z) and lateral (x) plane, shown in Fig. 2.

Insulation around the heater helped minimize heating of the surrounding water but the water outside of the plume inevitably warmed up, as is evident in the temperature along the x axis in Fig. 2. Typical scans were 20×20 mm, resulting in overall temperature rises of ~ 4 $^{\circ}\text{C}$ in the water surrounding the plume. This gradual temperature rise had an effect on the phase measurement and, left uncorrected, manifested alignment errors in the beam pattern following numerical back projection. The corresponding phase decrease due to the ambient temperature rise was corrected by determining the slope of the phase decrease and adding the incremental change at each position in the phase measurement of the heated scan. Following this procedure, the backpropagated beam position compared favorably with the backpropa-

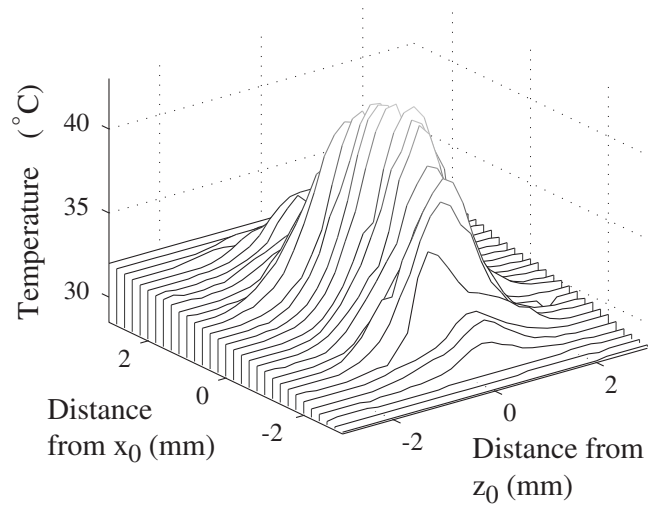


FIG. 2. Temperature profile across the x - z plane in the thermal plume measured with a thermocouple.

gated beam position from the reference scan. The ambient temperature rise also prevented use of a higher spatial resolution for the scan, as the lengthy scan duration would have resulted in a significantly lower difference between the plume and ambient water temperature. The impact of the 0.2 mm step size was evaluated by comparing the sound field with that measured with a 0.1 mm step size. The back-projected fields for both scans were nearly identical and showed no signs of spatial aliasing, demonstrating that the larger step size was sufficient.

The second phase-contrast setup is shown in Fig. 1(b). A cylindrical tissue phantom was constructed (63 mm length, 50 mm diameter) so that it would possess a higher sound speed than that of the surrounding water. In this arrangement, the phantom was positioned with the front face 18 mm from the transducer and the reference scan at the focus consisted of measuring the field through the homogeneous phantom with a short water path on either side. Two phase contrast scans were performed following excision of a water column in the phantom. The column was constructed by inserting a thin-walled brass pipe (3.18 mm outer diameter) into the phantom and water from the tank was flushed through the resulting cavity with a syringe. The first scan was conducted following creation of a horizontal column and the second scan was conducted following placement of a second, vertically oriented column, so that a progression of features could be visualized following analysis of the multiple scans. The phase contrast in this arrangement was due to the lower sound speed of the water in the column relative to the surrounding phantom matrix. In addition to placing multiple identifiable features in the phantom, the reduced sound speed in the column was expected to result in a phase column opposite to that of the thermal plume.

The phantom construction was based on a commonly used recipe³¹ with the sole difference of omitting graphite, as matching the attenuation was not of interest in this study. The phantom sound speed was measured to be $c_p = 1511$ m/s, using a time of flight method.³² Given the long scan times, it was anticipated that swelling of the phantom would be an issue; the phantom holder restricted the side of

the phantom but swelling of the top and bottom walls of the phantom towards the transducer and the hydrophone could impact the phase measurement over time. The phantom surface was treated in glutaraldehyde prior to measurement to minimize swelling³³ and multiple reference scans were conducted to investigate the potential impact of swelling on the phase. The phase at the focus was found to shift approximately 0.49 rad uniformly across the field. The impact of such a shift has the effect of uniformly increasing the phase angle contrast but as the reconstruction of an absolute temperature was not the goal of the phantom measurements, this small shift in phase was neglected. These two reference scans were also used as a control case before the water columns were introduced into the phantom to examine whether a significant phase contrast was revealed following back projection. No identifiable phase contrast feature was apparent and the phase difference across the image was negligible, with a standard deviation of 0.027 rad.

A second phase contrast orientation was also tested in the phantom measurements. The orientation exhibited in Fig. 1 sought to mimic an arrangement where the diagnostic transducer was oriented perpendicular to the therapeutic beam axis, so that the heated region encountered by the diagnostic beam was radially symmetric about the therapeutic beam axis. In a clinical setting where acoustic windows are limited it may be difficult to readily achieve such an arrangement; an ideal situation would instead have the diagnostic transducer positioned inline with the therapeutic transducer. Such an arrangement would eliminate registration issues regarding transducer alignment but would require certain assumptions about the geometry of the heated region in order to properly reconstruct the temperature rise. This arrangement was tested by changing the orientation of the water column so that its axis of symmetry was aligned with the transducer acoustic axis. A fresh, homogeneous phantom was used and a similar reference scan was conducted, followed by a scan with an on-axis water column placed throughout the cylindrical length of the phantom.

B. Simulation

The experiments described in the previous section were simulated to provide a practical means for testing the impact of the spatial dependence of the phase contrast feature. The phase contrast was simulated by creating an initial sound field and forward projecting it via Eq. (2) to the focus through a homogeneous reference medium with a sound speed of either water, for the thermal plume, or the measured phantom sound speed. The spatial distribution for the phase shift from the simulated plume was based on the measured temperature distribution of the peak temperature gradient shown in Fig. 2, whereas the phase shift for the simulated water column was based on the sound speed from the measured temperature of the tank water and the column diameter. The phase contrast scenario was tested by projecting the field along the axis of propagation to the position of the phase contrast and adding a phase shift equivalent to the experimental shift (this step was omitted for the reference field projection). The fields were then projected to the focus. Both

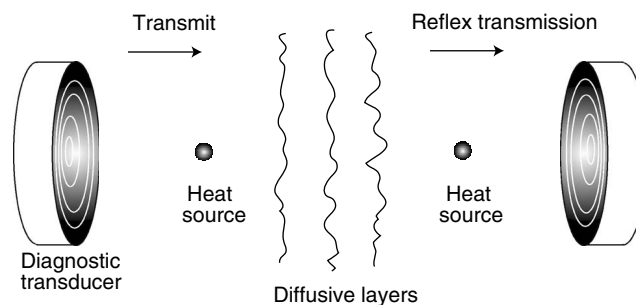


FIG. 3. Simulation arrangement for the phase contrast from a heat source with tissue effects present. The transducer used in the simulation was a 14-ring focused transducer with emission only from rings 8–11. The first case tested the arrangement shown here, whereas the second case did not have the heat source present upon transmit and the third case did not have the heat source present upon reflex transmission.

projected fields were backprojected to the position of the contrast region and the phase difference was tomographically reconstructed. The simulation was performed on a 78×78 mm grid with a 0.25-mm stepsize. The initial sound field was created by setting the amplitude on the 50-mm diameter transducer face to a constant value and the radius of curvature was simulated by incrementally shifting the initial phase depending on the radial position on the grid.

The feasibility of using RTI in a pulse–echo arrangement instead of through transmission was also simulated. The setup for this arrangement is shown in Fig. 3. The field was projected to the focus as described earlier, for the homogeneous reference case and with a phase contrast layer introduced along the path for the heated case. Near the focus, a diffusive phase shift layer was introduced to both fields in order to simulate the tissue structure which is expected to be responsible for scattering and reflecting the transmitted pulse back to the transducer. The field was then “reflected” back to the transducer by taking the complex conjugate of the phase and forward projecting the field to the equivalent position of the transducer, with a phase contrast layer again present for the heated field. The two fields were then back projected to the position of the contrast layer and reconstructed as before.

The phase shift of the diffusive layer was constructed by generating a random distribution for the phase. Physiologically the diffusion is not expected to necessarily follow a random distribution but rather a more structured pattern based on the tissue structure. The magnitude of the shift was based on measurements of the phase shift introduced by reflection off a tissue sample. Bovine muscle (~50 mm thick, store bought pot roast) was positioned at a 45° angle to the beam path approximately 50 mm from the transducer and the field was scanned with the hydrophone. The received pulse train at each position in the scan was analyzed to judge the extent of the phase shift from the expected phase of the transducer frequency. The reflected wave is a result of the initial reflection from the front tissue surface superimposed with energy reflected from a lateral part of the beam having transmitted into the tissue and subsequently scattered off the tissue structure towards the hydrophone. Multiple scans ex-

hibited a mean phase shift of ± 1 rad, so the random phase distribution for the simulated diffusive layer fell within ± 1 rad.

A potential drawback to using RTI in a pulse–echo arrangement is that the pulse is subject to heating on transmission and reflection, inducing a higher phase shift. Here it was hypothesized that a ring transducer may be employed such that the transmit pulse does not appreciably pass through the heated region but diffusive effects in the tissue sufficiently alter the beam pattern so that the pulse passes through the heated region only upon reflection. Such an arrangement would prevent the heated scan from experiencing up to double the phase shift but would require proper selection of the rings chosen for transduction. Interrogation of the heated region in the simulation was based on a 1.54 MHz concentric 14-ring focused transducer³⁴ (100-mm diameter, $f=1$), which will be available for future experimental study. Here, the heat source consisted of a spherical heat distribution rather than a linear plume distribution in order to more closely match the heat distribution resulting from a focused sound beam. This geometry resulted in a Gaussian distribution for the temperature radially away from the origin, rather than in just the lateral direction as in the plume arrangement.

A number of variables exist for simulating heating in this arrangement, such as number and position of transmit rings, position of the plume, number and position of the diffusive layers in the field. These variables were examined to evaluate the diffusion effect of tissue and three scenarios of heating were compared. Rings 8–11 were used for transmit and it was assumed that the entire returning sound field could be measured. Three diffusive layers were positioned 10 mm apart and 10 mm from the heat source, which was positioned 50 mm from the transducer. The heat source featured a 15 °C temperature rise relative to the rest of the medium, where $T_0=24$ °C. The sound speed dependence was modeled as that of water, corresponding to $c_0=1494$ m/s and $c_{\text{heat,max}}=1527$ m/s. The first scenario tested reconstruction of the temperature rise following propagation through the heat source and first diffusive layer on transmit, “reflection” off the second layer, and subsequent return through the third layer and heat source. The diffusion effects of the tissue for disrupting the beam focus was investigated in the second and third scenarios, where heating was applied only on the return or transmit paths, respectively. These two scenarios represent nonphysical situations but are included to demonstrate the feasibility of using a ring transducer and RTI for measuring temperature rise in tissue. The reference field for all scenarios differed only by omitting the phase contrast of the heat source, so that the same random phase distribution for the diffusive layer was used for both the reference and heated fields.

IV. RESULTS

A. Thermal plume

The temperature of the plume measured with the thermocouple is shown in Fig. 4(a). The positioning system scanned the thermocouple and hydrophone along the vertical y axis from -10 to 10 mm and marched across the lateral x

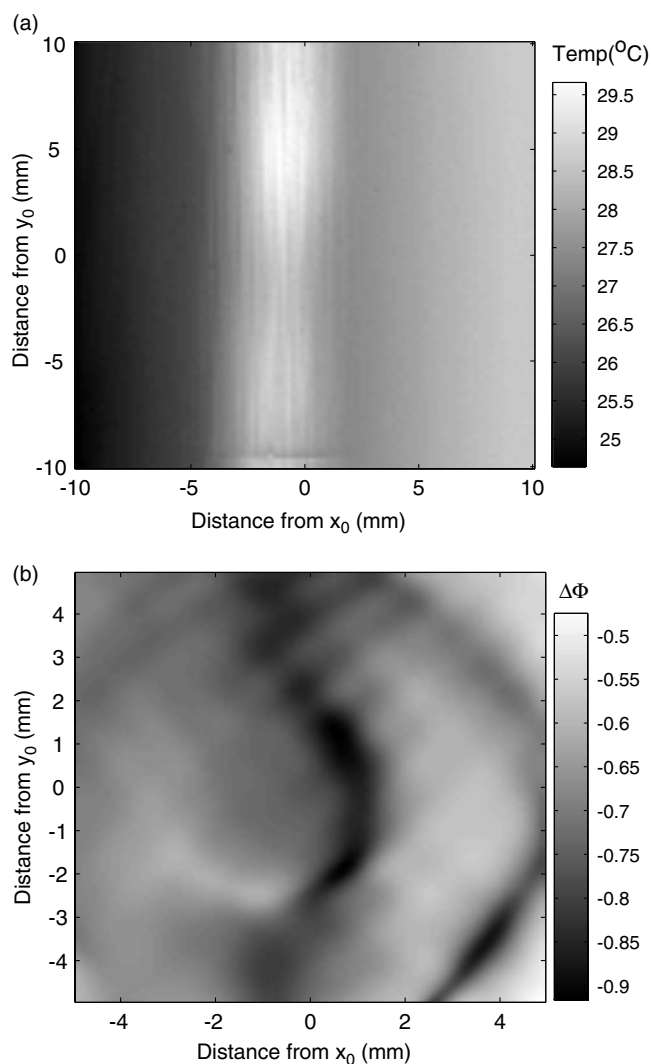


FIG. 4. (a) Temperature in the plume measured across the x - y plane with a thermocouple. The scan started at $x=y=-10$ mm and moved in 0.2 mm increments, scanning along the y axis before returning to $y=-10$ mm and moving to the next position on the x axis. (b) Phase difference between the heated and reference fields following back projection close to the plume.

axis from -10 to 10 mm. The temperature rise of the surrounding tank water rose approximately 3.5 °C over the ~ 4 h scan and the peak temperature rise of the plume was approximately 5 °C. Inspecting the temperature along the lateral (x) axis at any given vertical position revealed an approximately linear ambient temperature rise. Figure 4(b) shows the phase difference near the plume following back-projection of the two measured scans. The plume is identified by the slightly wavy decrease in the phase difference in the middle of the lateral axis. The difference between $\Delta\Phi$ in the plume ($x\sim 0$ mm) compared to the background $\Delta\Phi$ ($x\sim 3$ mm) was approximately 0.25 rad. The width of the measured plume was in good agreement with the width of the phase contrast plume.

The results from the tomographic reconstruction of the simulation and experimentally measured phase contrast are shown in Figs. 5(a) and 5(b), respectively. Figure 5(a) compares the temperature distribution on which the simulated phase contrast was based to the reconstructed temperature

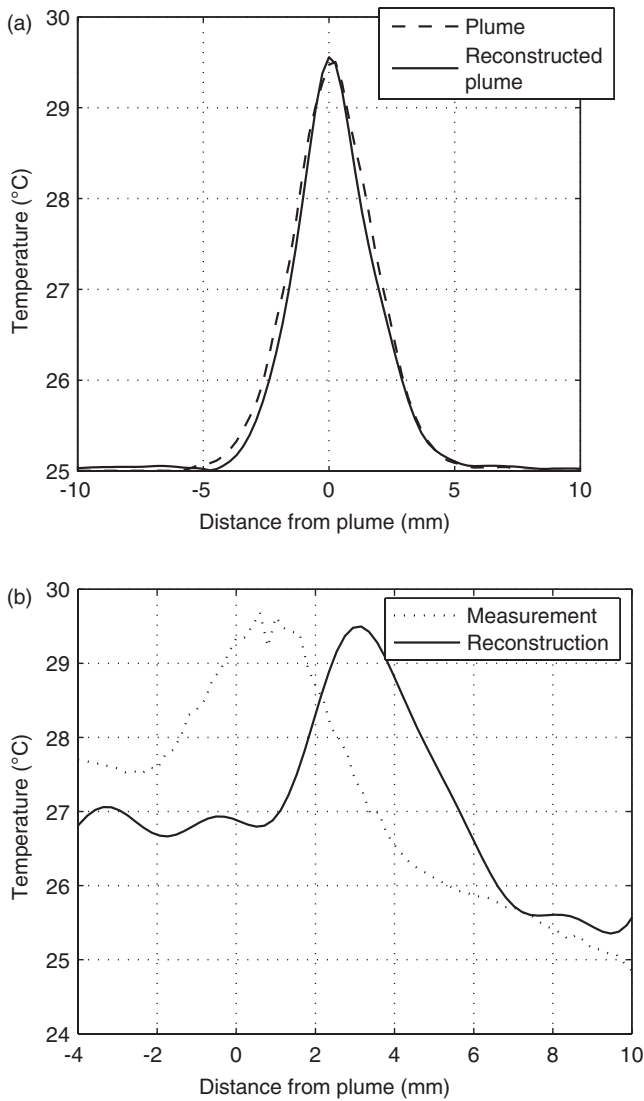


FIG. 5. (a) Comparison of the simulated plume temperature with the reconstructed temperature. (b) Comparison of the measured and estimated temperature following tomographic reconstruction.

distribution. The two curves agree well, with a peak temperature difference of $0.06\text{ }^{\circ}\text{C}$. Figure 5(b) shows the temperature measured with the thermocouple compared to the temperature following reconstruction of the phase contrast measured with the hydrophone. The two curves are shifted slightly along the lateral axis, most likely due to alignment errors between the thermocouple and hydrophone. Despite the lateral shift, the width of each curve agrees well and the peak temperature differs by only $0.2\text{ }^{\circ}\text{C}$.

B. Phantom

The phase difference of the water columns present in the phantom measurement is displayed in Fig. 6. The horizontal water column is evident in Fig. 6(a) as a horizontal increase in $\Delta\Phi$ positioned just above the focus. The water column had to be carefully excised so as to keep the phantom position faithful to its position in the reference scan, so the column had a slight angle compared to the lateral x axis and was angled slightly out of the x - y plane. In contrast to the ther-

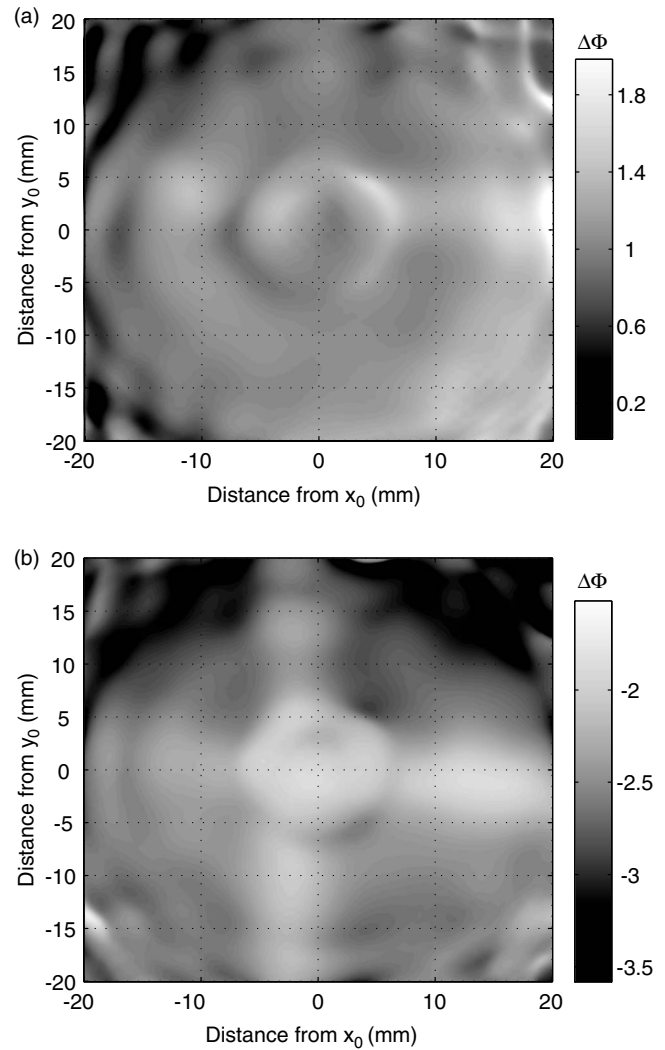


FIG. 6. (a) Phase difference between the phase contrast and reference fields following backprojection close to the horizontal water column in the phantom. (b) Phase difference following backprojection of the vertical and horizontal water column.

mal plume measurement where the phase decreased in the plume, the phase was higher in the water column due to the lower sound speed of the water compared to that of the phantom. The phase contrast of the horizontal column is not immediately clear in some parts of the image, where the image instead has a circular ripple effect. The addition of the vertical water column is visible along with the horizontal column in Fig. 6(b). Positioning errors in creating the vertical column were again evident as the two columns did not intersect, creating a region near the origin where the water path length with respect to the acoustic axis (z) was effectively doubled. Inspection of the phantom following measurement revealed that the two columns were separated by 7 mm along the z axis. In the non-overlapping portions of the columns the phase contrast is higher near the origin where the water path was longer.

Of note in the phantom results are the concentric ripples in the phase difference and the higher phase difference seen in the positive side of the horizontal column compared to the

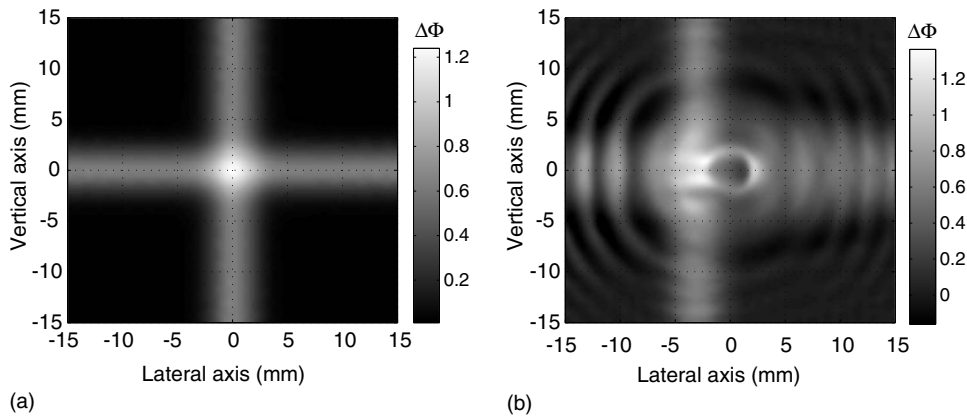


FIG. 7. (a) Backprojected phase difference between the simulated phase contrast and reference fields. Two overlapping water columns were used to produce the phase contrast. (b) Backprojected phase difference after separating the two columns by 7 mm and offsetting the vertical column from the origin of the lateral axis.

negative lateral side in both panels of Fig. 6. These features were examined in a simulation of the water columns present in the phantom. Figure 7(a) shows the simulated phase contrast for the water columns after back projection of the reference and phase contrast fields. Here the phase contrast of each water column was introduced so that the columns intersected in the x - y plane but with double the phase shift at the region of intersection near the origin (i.e., the phase shift from each column was added separately into the simulation). The resulting phase difference reveals straight, perpendicular columns with a maximum phase difference of 0.6 rad outside of the origin and approximately 1.2 rad at the origin. The simulation presented in Fig. 7(b) sought to more closely replicate the experiment, where the columns were slightly misaligned. In the experiment, the columns were not only positioned 7 mm apart from each other along the acoustic z axis but were also set at a small angle out of the x - y plane. This particular arrangement was simulated by positioning the columns 7 mm apart from one another along the z axis and the vertical column was offset from the lateral origin by 4 mm. The angle of each column out of the x - y plane was replicated by separating each column at the origin and positioning the two halves of the column 2 mm apart along the acoustic z axis. Figure 7(b) exhibits a ripple effect similar to Fig. 6 and the phase difference is no longer symmetric, with a higher contrast on the negative side of the horizontal column compared to the positive side. In addition, the phase difference in the offset case was similar to the experimental phase difference, ranging between 0.4 and 0.6 rad in the nonoverlapping regions.

The final experimental arrangement tested the detection of a water column placed along the acoustic axis. The phase difference from back projection of this measurement is shown in Fig. 8. The water column is immediately evident by the circular region centered about the lateral origin and $y = 7$ mm where the phase difference is highest. In contrast to the phase difference in the perpendicularly oriented water columns the phase difference here exhibits a sharp increase. The plateau effect seen in this phase contrast was most likely due to the geometry of the column in comparison to the perpendicular columns; the distance along the z axis over which the pulse traveled for the two media at any given position was the same, whereas the length of the path

through the water column in the perpendicular orientation changed smoothly across the column, steadily shifting the phase.

C. RTI simulation

Figure 9 shows results from the RTI simulation where tissue diffusion effects were examined. The temperature, following projection through the medium and reconstruction of the phase contrast, is plotted for the case of the diagnostic pulse experiencing heating on transmission and reflection and for the cases of propagation through the heated region solely on the return or transmit paths. Compared to the actual temperature rise of 1527 m/s, the realistic situation where roundtrip heating occurs resulted in a maximum reconstructed sound speed of 1534 m/s. The case of idealized heating only on the return trip resulted in a slightly more accurate maximum sound speed of 1531 m/s. The overall width of the heated region is slightly wider in the roundtrip heating case compared to the return-path heating but is nonetheless similar to the simulated heat geometry. Restricting heat deposition to the transmit path resulted in negligible phase contrast throughout the entire 2D field, as contrasted

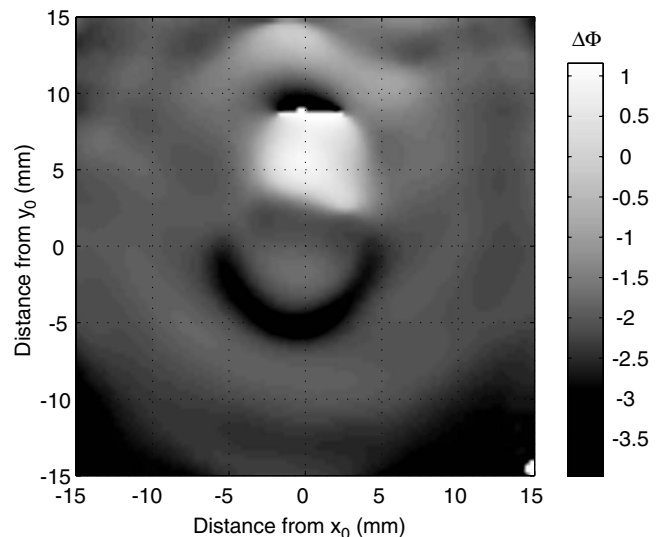


FIG. 8. Phase difference between an on-axis water column and reference field following backprojection.

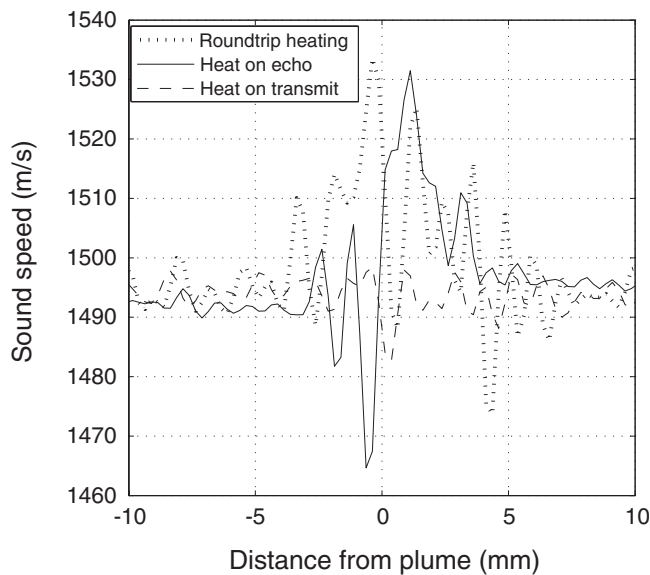


FIG. 9. Simulated comparison of the estimated sound speed for multiple heating arrangements in a pulse-echo setup. The case of heating on transmission and reflection (dotted) is compared with heating only on echo (solid) and heating only on transmit (dashed). The simulated maximum sound speed was 1527 m/s.

with the roundtrip heating simulation in Fig. 10. The phase contrast following heating on transmission and reflection is clearly visible near the origin of Fig. 10(a), whereas no such contrast can be seen in Fig. 10(b).

V. DISCUSSION

A thermal plume and a phantom intersected by water columns were separately used to produce a small phase change in the field, and analysis of the sound fields revealed accurate identification of the geometry and location of the phase contrast feature. The phase difference following back-projection and subtraction of the reference field matched the expected change, where the phase decreased for the temperature rise in the plume but increased for the lower sound speed in the water column. In addition, the temperature from the field reconstruction in Fig. 5 showed excellent agreement with the measured plume temperature. Both measurements featured an offset in the overall phase difference due to a shift in the field, either from bulk heating of the water or from swelling of the phantom. These problems underscore the difficulty of replicating heating from a HIFU source for a measurement that extends over several hours, and the need for a faster method of acquiring the field data. In the thermal case, the background water temperature rise was addressed by assuming a linear increase in temperature and the phase was adjusted accordingly. Accounting for swelling in the phantom was not as straightforward and reveals the issue that phase contrast measurements are susceptible to error due to target movement, an important factor to address in future work. However, phase measurements are attractive due to their low noise sensitivity, and combining the therapeutic and diagnostic transducers could assist in reducing problems stemming from target movement. The on-axis water column

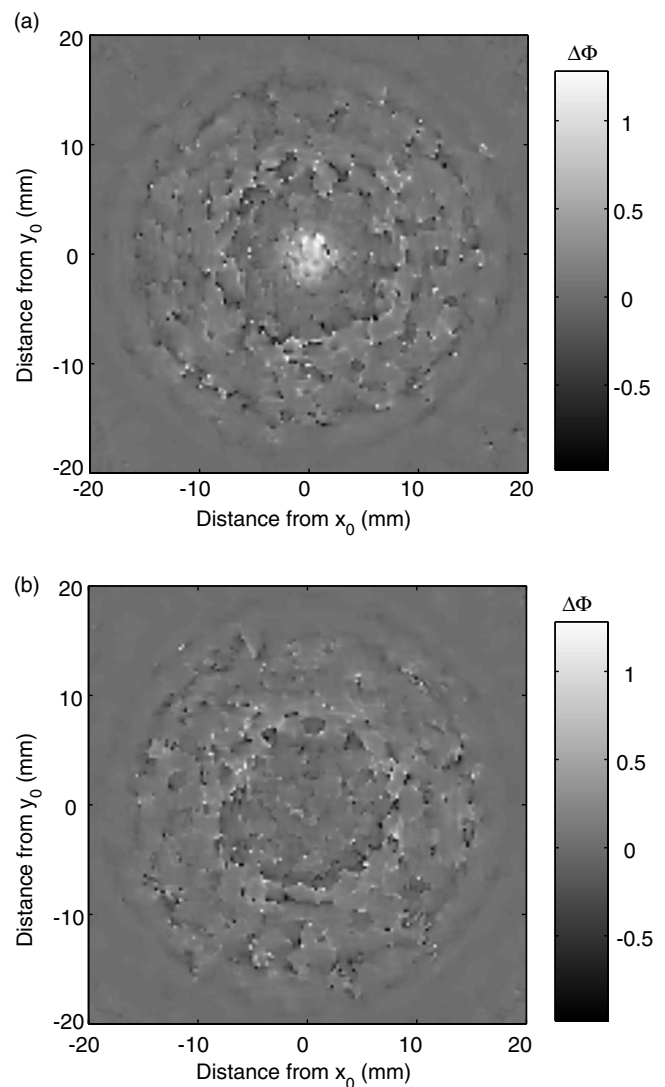


FIG. 10. Comparison of the simulated 2D phase difference for different heating arrangements in a pulse-echo setup when the outer rings of the transducer are used. Phase differences when heating is simulated (a) on transmission and reflex and (b) only on transmission.

measurement demonstrated that a co-axial arrangement of the diagnostic and therapeutic transducers is also feasible for detecting a phase change.

A couple of solutions exist for reducing the time required to measure the echo field, as a mechanical scan with a hydrophone is a lengthy process which would not be clinically feasible. An obvious, although hardware-intensive, solution is to use an array for the diagnostic transducer and acquire the rf signal from each element. This approach would require analog-to-digital conversion for each element to sufficiently reconstruct the field, and assumes that the entire sound field is contained within the geometrical footprint of the transducer so that the field can be properly back-projected. A second solution would be to use a phase-contrast filter as described by Clement and Hynynen.²⁶ This method would still require an array transducer in order to obtain sufficient spatial resolution but would not require a high sampling rate.

Simulation of the experimental setup revealed good agreement with the experimental results and helped explain some of the trends observed in the experimental data. The phase contrast in Fig. 6(b) is not uniform throughout the entire water column, as the contrast is greater for the right side of the horizontal column, as well as for the bottom portion (negative) of the vertical column, and the image shows ripples in the phase difference. Separating the simulated water columns along the acoustic z axis and offsetting the vertical column revealed a similar change in the phase contrast symmetry and emergence of concentric ripples in Fig. 7(b). These ripple artifacts have been well-documented in the ultrasound temperature imaging literature¹³⁻¹⁵ and are attributed to a refractive thermal lensing effect. Deviation of the phase difference away from the expected uniform, straight distribution demonstrates that alignment of the contrast feature relative to the sound beam can alter the perceived geometry of the feature, as distortion from refraction becomes increasingly pronounced when the contrast is positioned out-of-plane.

The present experimental configuration did not permit RTI, but simulation of such an arrangement with an approximation of the tissue effects showed that reflex transmission might be feasible in not only localizing the heat source in a 2D plane but measuring the temperature as well. The phase shift produced from multiple tissue layers was simulated by shifting the phase in a random distribution. Coupled with using only the outer rings of a concentric ring transducer, Fig. 10 demonstrates that the simulated tissue diffusion adequately served to alter the beam so that sufficient energy passed through the heated region only upon reflection. Although the simulation demonstrates that a ring-shaped beam pattern can be made sensitive to heating solely on the return path, the reconstructed sound speeds displayed in Fig. 10 drop below the reference speed at certain points. This is a nonphysical result which is believed to be an artifact from the simulation, due to error in the phase that occurs when the beam ring pattern amplitude is low. When all the rings are employed and the beam amplitude is sufficiently high throughout the entire heated region, heating is detected on both the transmission and reflection paths. Although this results in a higher sound speed, the sound speed is always above the reference speed, as the beam pattern does not contain nulls due to a ring pattern and consequent phase errors. Until the sound field reflected from the tissue structure following heat deposition is measured it will be difficult to know exactly how the tissue structure will affect the beam geometry along the entire pathlength. Nonetheless, if heating sufficiently alters the sound field on both the transmission and return paths at the very least a pulse-echo RTI setup should be effective at visualizing the 2D heat deposition.

As with most ultrasound thermographic methods, an additional factor in judging the success of this method is the underlying assumed relationship between temperature and sound speed. Multiple tissue layers of varying composition will affect not only the final temperature reconstruction but the backward projection as well. The use of ultrasound

phase-contrast transmission imaging for identifying multiple tissue types has been previously investigated²⁶ and remains an ongoing area of investigation.

The current method of tomographic reconstruction assumes radial symmetry, as integration of the phase difference is performed along a single direction. This assumption is fine for the current experimental arrangement but future setups where the heated region may be oblong rather than circular will require certain assumptions regarding the temperature distribution or a different approach for integrating the field. Left unaddressed, asymmetry in the temperature distribution would almost certainly result in miscalculation of the spatial extent and amplitude of the temperature. Once an array-based measurement system is developed, the acquisition time will decrease dramatically, which will allow the effect of alignment and lesion geometry on the reconstruction algorithm to be more easily investigated. Ultimately, the result from this system and analysis will be compared to MR thermometry measurements.

Other unknown factors include effects of cavitation on the propagation of the signal through a bubbly region. The sound speed is not expected to change appreciably due to the likely-low number of bubbles present but it is possible that scattering effects may preclude the diagnostic signal from propagating past and back through the bubbly region. However, a significant number of bubbles present in the field may suggest that boiling has already occurred, at which point the temperature will be significant and possibly above the target temperature.

Based on the sound speed dependence of water on temperature, the experimental and simulated investigations presented here were intended to show feasibility that the phase contrast obtained after backward projection and tomographic reconstruction can localize and measure a two-dimensional heat distribution. Experimental restrictions on measuring the sound field limited us to adopting a through-transmission setup, so although using an ultrasound through-transmission setup to measure temperature rise is not a novel endeavor, the techniques outlined and results obtained here incorporate a new approach that should translate well to a pulse-echo arrangement.

Many previous techniques¹³⁻¹⁹ rely on a beam-formed amplitude contrast image and correlation methods to determine the temperature change. These techniques can be easily corrupted by speckle noise, an effect which does not directly represent a physical feature in the region of interest. The approach described here gives a map of the sound field at the location of the feature which is of interest and may provide a more accurate description. Another advantage of this approach is that the temperature change is based on the phase information, which is less susceptible to noise and attenuation effects. Additionally, the computational time required to numerically project the field is relatively fast, promising a near-real-time imaging method. A number of issues still remain, such as motion and image registration, double-valued sound speeds at high temperatures, and thermal lensing effects, and will be addressed in future investigations. Many of these problems will be more easily addressed with an array-based acquisition system. The backprojection approach gives

some flexibility in observing how the field develops as it propagates, which may provide insight into accounting for thermal lensing effects. One solution to distinguishing between double-valued sound speeds at high temperatures would be to track the temperature change continuously by interleaving the diagnostic and therapeutic sonications. If the temperature change is sufficiently smooth and continuous, the direction of the sound speed change should indicate the direction of the temperature change.

VI. CONCLUSION

The ultrasound phase-contrast method described here obtained estimates in good agreement with the measured and observed phase contrast in the medium. The temperature contrast estimate was within 0.2 °C of the measured temperature and the water columns were clearly identified in the phantom measurements. Phase contrast was produced using both a thermal and sound speed change method, demonstrating that the technique is not limited solely to thermal features. Future application of these methods to a pulse-echo arrangement will allow the technique to be better suited for clinical adoption where acoustic access is limited, either with a perpendicular or parallel orientation to the therapeutic acoustic axis. The fast reconstruction time in conjunction with an array-based diagnostic transducer and phase contrast filter may allow for intermittent interrogation of the field while the therapeutic field is off, providing a continuous update of the temperature during treatment.

ACKNOWLEDGMENTS

Financial support for this research was provided by the NIH via Award No. U41 RR19703.

- ¹B. Quesson, J. A. de Zwart, and C. T. Moonen, "Magnetic resonance temperature imaging for guidance of thermotherapy," *J. Magn. Reson. Imaging* **12**, 525–533 (2000).
- ²N. McDannold, "Quantitative MRI-based temperature mapping based on the proton resonant frequency shift: Review of validation studies," *Int. J. Hyperthermia* **21**, 533–546 (2005).
- ³A. Kristensen and J. Dalen, "Acoustic estimation of size distribution and abundance of zooplankton," *J. Acoust. Soc. Am.* **80**, 601–611 (1986).
- ⁴M. Keidar, I. D. Boyd, and I. I. Beilis, "Electrical discharge in the Teflon cavity of a coaxial pulsed plasma thruster," *IEEE Trans. Plasma Sci.* **28**, 376–385 (2000).
- ⁵W. M. L. Morawitz, P. J. Sutton, P. F. Worcester, B. D. Cornuelle, J. F. Lynch, and R. Pawlowicz, "Three-dimensional observations of a deep convective chimney in the Greenland Sea during winter 1988/89," *J. Phys. Oceanogr.* **26**, 2316–2343 (1996).
- ⁶D. D. Iorio, D. Lemon, and R. Chave, "A self-contained acoustic scintillation instrument for path-averaged measurements of flow and turbulence with application to hydrothermal and bottom boundary layer dynamics," *J. Atmos. Ocean. Technol.* **22**, 1602–1617 (2005).
- ⁷F. A. Duck, *Physical Properties of Tissue* (Academic, London, 1990).
- ⁸K. Hynynen, N. I. Vykhodtseva, A. H. Chung, V. Sorrentino, V. Colucci, and F. A. Jolesz, "Thermal effects of focused ultrasound on the brain: Determination with MR imaging," *Radiology* **204**, 247–253 (1997).
- ⁹N. McDannold, C. M. Tempny, F. M. Fennessy, M. J. So, F. J. Rybicki, E. A. Stewart, F. A. Jolesz, and K. Hynynen, "Uterine leiomyomas: MR imaging-based thermometry and thermal dosimetry during focused ultrasound thermal ablation," *Radiology* **240**, 263–272 (2006).
- ¹⁰R. Seip and E. S. Ebbini, "Noninvasive estimation of tissue temperature response to heating fields using diagnostic ultrasound," *IEEE Trans. Biomed. Eng.* **42**, 828–839 (1995).
- ¹¹R. Maass-Moreno and C. A. Damianou, "Noninvasive temperature estimation in tissue via ultrasound echo-shifts. Part I. Analytical model," *J. Acoust. Soc. Am.* **100**, 2514–2521 (1996).
- ¹²R. Maass-Moreno, C. A. Damianou, and N. T. Sanghvi, "Noninvasive temperature estimation in tissue via ultrasound echo-shifts. Part II. In vitro study," *J. Acoust. Soc. Am.* **100**, 2522–2530 (1996).
- ¹³C. Simon, P. VanBaren, and E. S. Ebbini, "Two-dimensional temperature estimation using diagnostic ultrasound," *IEEE Trans. Ultrason. Ferroelectr. Freq. Control* **45**, 1088–1099 (1998).
- ¹⁴N. R. Miller, J. C. Bamber, and G. R. ter Haar, "Imaging of temperature-induced echo strain: Preliminary *in vitro* study to assess feasibility for guiding focused ultrasound surgery," *Ultrasound Med. Biol.* **30**, 345–356 (2004).
- ¹⁵M. Pernot, M. Tanter, J. Bercoff, K. R. Waters, and M. Fink, "Temperature estimation using ultrasonic spatial compound imaging," *IEEE Trans. Ultrason. Ferroelectr. Freq. Control* **51**, 606–615 (2004).
- ¹⁶M. D. Abolhassani, A. Norouzy, A. Takavar, and H. Ghanaati, "Noninvasive temperature estimation using digital images," *J. Ultrasound Med.* **26**, 215–222 (2007).
- ¹⁷A. Anand, D. Savery, and C. Hall, "Three-dimensional spatial and temporal temperature imaging in gel phantoms using backscattered ultrasound," *IEEE Trans. Ultrason. Ferroelectr. Freq. Control* **54**, 23–31 (2007).
- ¹⁸T. Varghese, J. A. Zagzebski, Q. Chen, U. Techavipoo, G. Frank, C. Johnson, A. Wright, and F. T. Lee, "Ultrasound monitoring of temperature change during radiofrequency ablation: Preliminary *in-vivo* results," *Ultrasound Med. Biol.* **28**, 321–329 (2002).
- ¹⁹T. Varghese and M. J. Daniels, "Real-time calibration of temperature estimates during radiofrequency ablation," *Ultrason. Imaging* **26**, 185–200 (2004).
- ²⁰R. L. King, G. T. Clement, S. Maruvada, and K. Hynynen, "Preliminary results using ultrasound transmission for image-guided thermal therapy," *Ultrasound Med. Biol.* **29**, 293–299 (2003).
- ²¹K. Mizutani, K. Nishizaki, K. Nagai, and K. Harakawa, "Measurement of temperature distribution in space using ultrasound computerized tomography," *Jpn. J. Appl. Phys., Part 1* **36**, 3176–3177 (1997).
- ²²E. Ishikawa, K. Mizutani, and K. Nagai, "Fast method for visualization of temperature distribution using acoustic computerized tomography," *Jpn. J. Appl. Phys., Part 1* **40**, 5446–5449 (2001).
- ²³P. S. Green and M. Ardit, "Ultrasonic reflex imaging," *Ultrason. Imaging* **7**, 201–214 (1985).
- ²⁴P. S. Green, J. S. Ostrem, and T. K. Whitehurst, "Combined reflection and transmission ultrasound imaging," *Ultrasound Med. Biol.* **17**, 283–289 (1991).
- ²⁵D. Rallan, N. L. Bush, J. C. Bamber, and C. C. Harland, "Quantitative discrimination of pigmented lesions using three-dimensional high-resolution ultrasound reflex transmission imaging," *J. Invest. Dermatol.* **127**, 189–195 (2007).
- ²⁶G. T. Clement and K. Hynynen, "Ultrasound phase-contrast transmission imaging of localized thermal variation and the identification of fat/tissue boundaries," *Phys. Med. Biol.* **50**, 1585–1600 (2005).
- ²⁷V. A. Del Grosso, and C. W. Mader, "Speed of sound in pure water," *J. Acoust. Soc. Am.* **52**, 1442–1446 (1972).
- ²⁸P. R. Stepanishen and K. C. Benjamin, "Forward and backward projection of acoustic fields using FFT methods," *J. Acoust. Soc. Am.* **71**, 803–812 (1982).
- ²⁹D. Liu and R. Waag, "Propagation and backpropagation for ultrasonic wavefront design," *IEEE Trans. Ultrason. Ferroelectr. Freq. Control* **44**, 1–13 (1997).
- ³⁰A. C. Kak, and M. Slaney, *Principles of Computerized Tomographic Imaging* (IEEE Press, Piscataway, NJ, 1988), Chap. 3, pp. 49–60.
- ³¹M. M. Burlew, E. L. Madsen, J. A. Zagzebski, and R. A. Banjavic, "A new ultrasound tissue-equivalent material," *Radiology* **134**, 517–520 (1980).
- ³²J. C. Bamber, "Ultrasonic properties of tissues," in *Ultrasound in Medicine*, edited by F. A. Duck, A. C. Baker, and H. C. Starritt, (IOP Publishing, Philadelphia, 1998), pp. 68–69.
- ³³L. K. Ryan, and F. S. Foster, "Tissue equivalent vessel phantoms for intravascular ultrasound," *Ultrasound Med. Biol.* **23**, 261–273 (1997).
- ³⁴T. Fjield, X. Fan, and K. Hynynen, "A parametric study of the concentric-ring transducer design for MRI guided ultrasound surgery," *J. Acoust. Soc. Am.* **100**, 1220–1230 (1996).